

# Fe XI emission lines in a high resolution extreme ultraviolet active region spectrum obtained by SERTS

F. P. Keenan<sup>1</sup>, K. M. Aggarwal<sup>1</sup>, R. S. I. Ryans<sup>1</sup>, R. O. Milligan<sup>1,2</sup>, D. S. Bloomfield<sup>1</sup>, J. W. Brosius<sup>2,3</sup>, J. M. Davila<sup>2</sup> and R. J. Thomas<sup>2</sup>

F.Keenan@qub.ac.uk

## ABSTRACT

New calculations of radiative rates and electron impact excitation cross sections for Fe XI are used to derive emission line intensity ratios involving  $3s^23p^4-3s^23p^33d$  transitions in the 180–223 Å wavelength range. These ratios are subsequently compared with observations of a solar active region, obtained during the 1995 flight of the *Solar EUV Research Telescope and Spectrograph* (SERTS). The version of SERTS flown in 1995 incorporated a multilayer grating that enhanced the instrumental sensitivity for features in the  $\sim 170$ –225 Å wavelength range, observed in second-order between 340 and 450 Å. This enhancement led to the detection of many emission lines not seen on previous SERTS flights, which were measured with the highest spectral resolution (0.03 Å) ever achieved for spatially resolved active region spectra in this wavelength range. However, even at this high spectral resolution, several of the Fe XI lines are found to be blended, although the sources of the blends are identified in the majority of cases. The most useful Fe XI electron density diagnostic line intensity ratio is  $I(184.80 \text{ \AA})/I(188.21 \text{ \AA})$ . This ratio involves lines close in wavelength and free from blends, and which varies by a factor of 11.7 between  $N_e = 10^9$  and  $10^{11} \text{ cm}^{-3}$ , yet shows little temperature sensitivity. An unknown line in the SERTS spectrum at 189.00 Å is found to be due to Fe XI, the first time (to our knowledge) this feature has been identified in the solar spectrum. Similarly, there are new identifications of the Fe XI 192.88, 198.56 and 202.42 Å features, although the latter two are blended with S VIII/Fe XII and Fe XIII, respectively.

*Subject headings:* Atomic data – Sun: active region – Ultraviolet: spectra

---

<sup>1</sup>Department of Pure and Applied Physics, Queen’s University Belfast, Belfast, BT7 1NN, Northern Ireland, U.K.

<sup>2</sup>Laboratory for Astronomy and Solar Physics, Code 682, NASA’s Goddard Space Flight Center, Greenbelt, MD 20771

<sup>3</sup>Department of Physics, The Catholic University of America, Washington, DC 20064

## 1. Introduction

Emission features arising from transitions in Fe XI are routinely detected in solar extreme ultraviolet spectra (see, for example, Dere 1978; Thomas & Neupert 1994). The diagnostic potential of these lines for determining the electron density in the emitting plasma was first demonstrated by Kastner & Mason (1978). Since then, several authors have produced theoretical line ratios for Fe XI applicable to solar spectra (see Bhatia, Doschek, & Eissner 2002 and references therein).

In this paper we present theoretical Fe XI line ratios for a range of electron temperatures and densities, generated using the most recent calculations of radiative rates and R-matrix electron impact excitation cross sections. We subsequently compare these line ratios with active region observations obtained with the *Solar EUV Research Telescope and Spectrograph* (SERTS) sounding rocket experiment. Specifically, we employ the SERTS dataset obtained during the 1995 flight, when the instrument incorporated a multilayer-coated toroidal diffraction grating that enhanced its sensitivity for features in the  $\sim 170\text{--}225$  Å wavelength range, observed in second-order between 340 and 450 Å. This led to the detection of many emission lines not seen on previous SERTS flights (Thomas & Neupert 1994; Brosius et al. 1996), and provided the highest spectral resolution (0.03 Å) ever achieved for spatially resolved active region spectra in this wavelength range (Brosius, Davila, & Thomas 1998). Hence this SERTS dataset allows us to undertake the most comprehensive analysis to date of the solar Fe XI spectrum in the 170–225 Å wavelength region.

## 2. Observational Data

The solar spectrum analysed in the present paper is that of active region NOAA 7870, recorded on Eastman Kodak 101–07 emulsion by SERTS during a rocket flight on 1995 May 15 at 1800 UT (Brosius et al. 1998). SERTS first flew in 1989 (Neupert et al. 1992; Thomas & Neupert 1994), and carried a standard gold-coated toroidal diffraction grating. It observed hundreds of first-order emission lines in the 235–450 Å wavelength range, as well as dozens of features spanning 170–225 Å, which appeared in second-order between 340 and 450 Å. The version of SERTS flown in 1991 and 1993 (Brosius et al. 1996) carried a multilayer-coated diffraction grating that enhanced the instrumental efficiency in the first-order wavelength range. However, as noted in § 1, the version flown in 1995 incorporated a multilayer grating that enhanced the instrumental sensitivity for second-order features. The SERTS 1995 active region spectrum therefore provides the best observations for investigating solar Fe XI emission lines in the 170–225 Å wavelength region. Further details of the observations, and the wavelength and absolute flux calibration procedures employed in the data reduction,

may be found in Brosius et al. (1998).

We have searched for Fe XI emission lines in the SERTS spectrum, using the identifications of Jupén, Isler, & Träbert (1993) and the NIST database<sup>1</sup>, as well as previous solar detections where available (for example, those by Behring, Cohen, & Feldman 1972; Behring et al. 1976). In Table 1 we list the Fe XI transitions found in the spectrum, along with the measured wavelengths. We also note possible blending species or alternative identifications, as suggested by Brosius et al. (1998) in their original line list for the active region spectrum,

Intensities and line widths (FWHM) of the Fe XI features are given in Table 2, along with the associated  $1\sigma$  errors. These were determined by using the spectrum synthesis package DIPSO (Howarth, Murray, & Mills 1994) to fit Gaussian profiles to the observations. Uncertainties in these measurements have been determined using methods discussed in detail by Thomas & Neupert (1994). In Figures 1–4 we plot portions of the SERTS spectrum containing the Fe XI features, to show the quality of the observational data. We note that each SERTS spectrum exhibits a background level due to film fog, scattered light and actual solar continuum. The background was calculated using methods detailed in Thomas & Neupert (1994) and Brosius et al. (1998), and then subtracted from the initial spectrum, leaving only an emission line spectrum (with noise) on a zero base level. It is this zero base level which is shown in Figures 1–4. We note that some of the measured Fe XI emission lines, such as the 184.80 Å transition (Figure 1), have line intensities comparable to the noise fluctuations. In these instances the reality of the line was confirmed by a visual inspection of the original SERTS film.

### 3. Theoretical Line Ratios

The model ion for Fe XI consisted of the 24 energetically lowest LS states, namely  $3s^23p^4$   $^3P$ ,  $^1D$ ,  $^1S$ ;  $3s3p^5$   $^3P$ ,  $^1P$ ;  $3s^23p^3(^4S)3d^5D$ ;  $3s^23p^3(^2D)3d^3D$ ,  $^3F$ ,  $^1S$ ,  $^3G$ ,  $^1G$ ;  $3s^23p^3(^2P)3d^1D$ ,  $^3D$ ,  $^3P$ ,  $^3F$ ,  $^1F$ ;  $3s^23p^3(^2D)3d^3S$ ,  $^3P$ ,  $^1P$ ;  $3s^23p^3(^4S)3d^3D$ ;  $3s^23p^3(^2D)3d^1D$ ,  $^1F$ ,  $^1P$ ;  $3p^6$   $^1S$ , yielding a total of 48 fine-structure levels. Experimental energy levels, which are only available for a relatively small number (20) of Fe XI states, were obtained from Shirai et al. (1990) and Jupén et al. (1993). For the remaining values the theoretical results of Aggarwal & Keenan (2003a) were adopted. Test calculations including higher-lying  $3s^23p^34l$  levels were found to have a negligible effect on the theoretical line ratios considered in this paper.

The electron impact excitation cross sections adopted in the present paper are the

---

<sup>1</sup><http://physics.nist.gov/PhysRefData/>

recent R-matrix calculations of Aggarwal & Keenan (2003b), while Einstein A-coefficients for allowed and intercombination lines were obtained from Aggarwal & Keenan (2003a). These A-values are similar to those of Deb & Tayal (1998) and Bhatia & Doschek (1996), apart from transitions involving levels 39 ( $3s^23p^3(^2D)3d^3P_1$ ) and 41 ( $3s^23p^3(^2D)3d^1P_1$ ), where there are large discrepancies. It appears that these levels have been interchanged in the previous two calculations, as agreement is restored if Aggarwal & Keenan (2003a) reclassify the A-values relating to level 39 as belonging to level 41, and vice-versa. However we note that Aggarwal & Keenan (2003a) performed several test calculations, involving configuration interaction with different orbitals and configurations, and in each instance obtained the same energy level ordering. They are hence confident of the ordering of the levels of their calculations.

Radiative rates for forbidden transitions have also been taken from the work of Aggarwal & Keenan (2003a), although the data were not included in the published paper for conciseness. They are available from the authors on request. However we note that the results are very similar to those calculated by others, such as Bhatia et al. (2002). Proton impact excitation is only important for transitions within the  $3s^23p^4\ ^3P$  ground term, and in the present analysis we have employed the calculations of Landman (1980).

Using the above atomic data, in conjunction with a recently updated version of the statistical equilibrium code of Dufton (1977), relative Fe XI level populations and hence emission line strengths were calculated as a function of electron temperature ( $T_e$ ) and density ( $N_e$ ). Details of the procedures involved and approximations made may be found in Dufton (1977) and Dufton et al. (1978).

In Figures 5–9 we plot the theoretical emission line ratios

$$R_1 = I(180.38 \text{ \AA})/I(188.21 \text{ \AA}),$$

$$R_2 = I(181.13 \text{ \AA})/I(188.21 \text{ \AA}),$$

$$R_3 = I(182.17 \text{ \AA})/I(188.21 \text{ \AA}),$$

$$R_4 = I(184.80 \text{ \AA})/I(188.21 \text{ \AA}),$$

$$R_5 = I(188.30 \text{ \AA})/I(188.21 \text{ \AA}),$$

$$R_6 = I(189.00 \text{ \AA})/I(188.21 \text{ \AA}),$$

$$R_7 = I(189.19 \text{ \AA})/I(188.21 \text{ \AA}),$$

$$R_8 = I(202.42 \text{ \AA})/I(188.21 \text{ \AA}),$$

and

$$R_9 = I(223.00 \text{ \AA})/I(188.21 \text{ \AA}),$$

as a function of electron density at the temperature of maximum Fe XI fractional abundance in ionization equilibrium,  $T_e = T_{max} = 10^{6.1}$  K, plus  $\pm 0.2$  dex about this value, where the fractional abundance has fallen to  $N(\text{Fe XI})/N(\text{Fe}) \leq 0.06$  (Mazzotta et al. 1998).

We note that the ratios

$$R_{10} = I(189.72 \text{ \AA})/I(188.21 \text{ \AA}),$$

$$R_{11} = I(192.88 \text{ \AA})/I(188.21 \text{ \AA}),$$

$$R_{12} = I(193.51 \text{ \AA})/I(188.21 \text{ \AA}),$$

and

$$R_{13} = I(198.56 \text{ \AA})/I(188.21 \text{ \AA}),$$

have the same temperature and density dependence as  $R_5$  or  $R_7$ , owing to common upper levels, but with

$$R_{10} = 0.875 \times R_7,$$

$$R_{11} = 0.337 \times R_5,$$

$$R_{12} = 0.0929 \times R_5,$$

and

$$R_{13} = 0.438 \times R_7.$$

Similarly, the branching ratio

$$R_{14} = I(192.81 \text{ \AA})/I(188.21 \text{ \AA}),$$

is predicted to have the constant value  $R_{14} = 0.190$ , owing to common upper levels.

The transitions corresponding to the wavelengths listed above are given in Table 1. Given errors in the adopted atomic data of typically  $\pm 10\%$  (see the references above), we would expect the theoretical ratios to be accurate to better than  $\pm 20\%$ .

The ratios in Figures 5–9 are given relative to the 188.21  $\text{\AA}$  transition, as this feature is the cleanest and most reliably detected Fe XI emission line in the SERTS spectrum (see Figures 1–4). We have confirmed this via a search of line lists, such as the Atomic Line List of van Hoof<sup>2</sup>, and also by generating a synthetic active region spectrum using the latest

---

<sup>2</sup><http://star.pst.qub.ac.uk/~pvh/>

version (4.2) of the CHIANTI database (Dere et al. 1997; Young et al. 2003). No transitions in first or second-order with intensities  $> 3\%$  that of the 188.21 Å line were found. However, we note that theoretical results involving any line pair are available from one of the authors (F.Keenan@qub.ac.uk) on request.

An inspection of the figures reveals that several of the line ratios, in particular  $R_3$  and  $R_4$ , are very sensitive to variations in the electron density. However most of the ratios are relatively insensitive to the adopted electron temperature. The strong  $N_e$ -dependence of ratios such as  $R_3$  and  $R_4$ , combined with their temperature insensitivity, make them potentially useful density diagnostics for the Fe XI emitting region of a plasma.

We note that the current line ratios can differ by up to typically 20–30% with other recent calculations. For example, at  $T_e = 10^{6.1}$  K and  $N_e = 10^8$  cm $^{-3}$ , we calculate  $R_1 = 1.8$  and  $R_3 = 0.18$ , compared to  $R_1 = 2.2$  and  $R_3 = 0.26$  from the latest version of CHIANTI. These discrepancies are due primarily to the adoption of the Aggarwal & Keenan (2003b) excitation rates in the present analysis, as opposed to the results of Bhatia & Doschek (1996) and Gupta & Tayal (1999a,b) adopted by previous authors (see Aggarwal & Keenan 2003b for more details).

#### 4. Results and Discussion

In Table 3 we summarise the observed Fe XI emission line intensity ratios, along with the associated  $1\sigma$  errors. Also shown in the table are the theoretical results from Figures 5–9 at the temperature of maximum fractional abundance in ionization equilibrium for Fe XI,  $T_{max} = 10^{6.1}$  K (Mazzotta et al. 1998), and an electron density of  $N_e = 10^{9.4}$  cm $^{-3}$ . This density was derived for the SERTS active region from emission line ratios in Fe X, Fe XIII and Fe XIV (Brosius et al. 1998), which have similar values of  $T_{max}$  to Fe XI ( $10^6$ – $10^{6.3}$  K). Hence the Fe X, Fe XIII and Fe XIV densities should reflect that of the Fe XI emitting plasma in the active region. We note that Fe XII line ratios in the active region imply significantly higher values of density ( $N_e \simeq 10^{10}$  cm $^{-3}$ ), but these have not been adopted in the present work as they are inconsistent with the other Fe ions, and may indicate a problem with the Fe XII diagnostics. However, changing the theoretical line ratios in Table 3 to values for  $N_e \simeq 10^{10}$  cm $^{-3}$  would not significantly alter the discussion below. For  $R_{14}$ , which is predicted to be  $N_e$ -insensitive, the theoretical result in Table 3 is the value listed in § 3. Error bars for all the theoretical ratios are based on the estimated  $\pm 20\%$  accuracy of the calculations (see § 3).

An inspection of Table 3 reveals excellent agreement between theory and observation

for the  $R_4$  and  $R_{14}$  ratios, indicating that the 184.80 and 192.81 Å lines are well detected and free from blends. More importantly, these results imply that  $R_4$  may be employed with confidence as an  $N_e$ -diagnostic. It should be particularly useful over the  $N_e = 10^9$ – $10^{11}$  cm $^{-3}$  interval, where it varies by a factor of 11.7 and yet shows little temperature sensitivity (see Figure 7).

For the ratios  $R_2$ ,  $R_3$  and  $R_{10}$ , agreement between theory and observation is less satisfactory, but the calculated and experimental measurements do overlap within the uncertainties. Hence we can state that the 181.13, 182.17 and 189.72 Å emission lines appear to be free from blends, especially as an inspection of line lists and the synthetic active region spectrum from CHIANTI reveals no likely candidates in first or second-order. From Figure 6, the  $R_3$  ratio should provide a reasonably good  $N_e$ -diagnostic, varying by a factor of 2.5 between  $N_e = 10^9$  and  $10^{11}$  cm $^{-3}$ . However on the basis of the present analysis it is advised that more weight should be given to results from  $R_4$ .

In the cases of  $R_1$  and  $R_{12}$ , the measured line ratios are much larger than the theoretical values, confirming that the 180.38 and 193.51 Å lines are badly blended. Brosius et al. (1998) note that the 180.38 Å line is blended with an Fe XVI transition observed at 360.76 Å in first-order. However these authors list the 193.51 Å feature as being due entirely to Fe XII. This is effectively the case, as Fe XI contributes less than 2% to the total 193.51 Å line intensity.

Dere et al. (1997) list the 188.30 Å line as being due to the  $3s^23p^4\ ^3P_2$ – $3s^23p^3(^2D)3d\ ^1P_1$  transition (equivalent to  $3s^23p^4\ ^3P_2$ – $3s^23p^3(^2D)3d\ ^3P_1$  in our notation, as we interchange the  $^3P_1$  and  $^1P_1$  levels; see § 3). They preferred this to the  $3s^23p^4\ ^3P_2$ – $3s^23p^3(^2D)3d\ ^3S_1$  identification of Jupén et al. (1993), as the latter was predicted to be weak. However we calculate that the intensity of the  $^3P_2$ – $^3S_1$  line should be 21% that of the 188.21 Å feature, slightly larger than the  $^3P_2$ – $^3P_1$  intensity which is predicted to be 19% of  $I(188.21\ \text{Å})$ . Hence we believe that the 188.30 Å feature is due to the  $^3P_2$ – $^3S_1$  transition, as classified by Jupén et al., although the disagreement between theory and observation for  $R_5$  implies that the line is blended, as previously noted by Brosius et al. (1998). There are no obvious blending species, although Brosius et al. point out that Kelly (1987) lists an Si line from an undetermined ionization stage at 188.3 Å. Also, Dere (1978) lists a line at 376.61 Å which would be the second-order detection of a feature at 188.31 Å. However Thomas & Neupert (1994) identify this as a Mg V transition, which is very weak in the 1989 SERTS active region dataset, and hence is unlikely to be responsible for the blend. This is confirmed by the CHIANTI synthetic spectrum, which indicates that the Mg V line should have an intensity  $< 10^{-5}$  that of the Fe XVI 360.76 Å feature, observed by SERTS at 180.38 Å with  $I = 3440$  erg cm $^{-2}$  s $^{-1}$  sr $^{-1}$ . Hence the predicted intensity of the Mg V transition is  $< 0.01\%$  that of the 188.30 Å feature

in Table 2.

Brosius et al. (1998) have tentatively associated the 189.19 Å line in the SERTS active region spectrum as being due to Fe XI, although the wavelength of the feature is higher than previously measured (189.13 Å). Kelly (1987) lists an Mn IX line at 189.16 Å and a Ni XV transition at 189.21 Å. However, a comparison of the observed and theoretical  $R_7$  ratios from Table 3 indicates that blending is probably not responsible for any wavelength discrepancy, as the measured ratio is actually smaller than the calculated value. The SERTS wavelength measurement should be accurate to  $\pm 0.01$  Å or better (see Figure 3 and Brosius et al.), and as noted in § 2 this is the highest resolution solar active region spectrum obtained over the 170–225 Å wavelength region. Hence we are confident of the wavelength measurement for the Fe XI line, and the discrepancy may be due to inaccuracies in previous determinations from lower quality data.

The good agreement between theory and observation for  $R_6$  confirms that the 189.00 Å feature, previously unidentified in the SERTS spectrum, is due to Fe XI. To our knowledge, this is the first time this Fe XI transition has been identified in the solar spectrum. Similarly, our results for  $R_{11}$  indicate that the 192.88 Å feature must have a significant contribution from Fe XI, and is not totally due to Ca XVII as suggested by Brosius et al. (1998). The observed  $R_{11}$  ratio is somewhat larger than theory (although they agree within the error bars), so that Ca XVII may make a 30–50% contribution to the line blend. Once again, to our knowledge this is the first time this Fe XI line has been identified in the solar spectrum.

Brosius et al. (1998) list the 223.00 Å line as a blend of Fe XI and Ca XVII. However our calculations for  $R_9$  show that the Fe XI contribution is negligible, while the intensity of the Ca XVII 223.00 Å transition is predicted to be less than 1% that of the 192.88 Å line (Dufton et al. 1983), ruling out a Ca XVII identification. A more likely candidate for the 223.00 Å feature is the  $2s^2S_{1/2}-2p^2P_{3/2}$  resonance line of Cr XXII, suggested by both Dere (1978) and Dufton et al. Support for this comes from the CHIANTI synthetic spectrum, which predicts the  $2s^2S_{1/2}-2p^2P_{1/2}$  line of Cr XXII at 279.74 Å and an intensity ratio  $I(279.74 \text{ Å})/I(223.00 \text{ Å}) = 0.42$ . There is indeed an unidentified feature in the SERTS spectrum at this wavelength, with  $I(279.74 \text{ Å})/I(223.00 \text{ Å}) = 0.55 \pm 0.21$ . The presence of two features at the predicted wavelengths of the Cr XXII lines and with the correct intensity ratio may be a coincidence, but this must be considered unlikely. Hence we believe that the 223.00 and 279.74 Å features are the two components of the Cr XXII doublet. Furthermore, the detection of the resonance lines of a highly ionized species such as Cr XXII in the SERTS spectrum implies that Ca XVII probably does make a significant contribution to the 192.88 Å feature (see above), as the Ca XVII transition is also a strong resonance line, and the solar abundance of Ca is larger than that for Cr.

The 198.56 and 202.42 Å features are listed as being due to S VIII/Fe XII and Fe XIII, respectively, by Brosius et al. (1998). However our calculations for R<sub>13</sub> and R<sub>8</sub> reveal that Fe XI makes significant (~50%) contributions to both the 198.56 and 202.42 Å line fluxes. Once again, this is the first time (to our knowledge) that these Fe XI transitions have been identified in the solar spectrum.

One concern of the present work is our failure to detect the  $3s^23p^4\ ^3P_2-3s^23p^3(^2D)3d\ ^3P_1$  transition at 184.70 Å (Jupén et al. 1993), although we have identified the  $^3P_1-^3P_1$  and  $^3P_0-^3P_1$  lines at 189.19 and 189.72 Å, respectively. The 184.70 Å transition is predicted to have an intensity about 20% that of the 188.21 Å feature. However an inspection of the SERTS dataset in this wavelength region (Figure 1) reveals no convincing detection.

Clearly, further research on the Fe XI spectrum is required. In particular, we believe that high spectral resolution observations of magnetically-confined tokamak plasmas could provide an enormous contribution to understanding solar Fe XI emission. The physical conditions in such plasmas are quite similar to those found in the solar transition region and corona, but can be independently measured to a high degree of accuracy, which in turn allows theoretical line strengths to be reliably predicted. Also, emission lines from species other than the element under consideration will generally not play an important role in a tokamak spectrum, greatly reducing the amount of blending. As result, tokamak observations have frequently been employed to test astrophysical diagnostic calculations, and to help in the identification of emission lines in solar spectra (see, for example, Keenan et al. 2000, 2003). Through a collaboration with the UKAEA Culham Laboratory, we have access to an extensive range of tokamak spectral observations, including those from the *Joint European Torus* (JET). In the future we therefore plan to search the JET and other tokamak databases for suitable Fe XI spectra.

K.M.A. and R.S.I.R. acknowledge financial support from the EPSRC and PPARC Research Councils of the United Kingdom. R.O.M. and D.S.B are grateful to the Department of Education and Learning (Northern Ireland) for the award of studentships, while the latter also acknowledges financial support from NASA’s Goddard Space Flight Center. The SERTS rocket programme is supported by RTOP grants from the Solar Physics Office of NASA’s Space Physics Division. JWB acknowledges additional NASA support under grant NAG5–13321. F.P.K. is grateful to AWE Aldermaston for the award of a William Penney Fellowship. The authors thank Peter van Hoof for the use of his Atomic Line List.

## REFERENCES

- Aggarwal, K. M., & Keenan, F.P. 2003a, MNRAS, 338, 412
- Aggarwal, K. M., & Keenan, F. P. 2003b, A&A, 399, 799
- Behring, W. E., Cohen, L., & Feldman, U. 1972, ApJ, 175, 493
- Behring, W. E., Cohen, L., Feldman, U., & Doschek, G. A. 1976, ApJ, 203, 521
- Bhatia, A. K., & Doschek, G. A. 1996, At. Data Nucl. Data Tables, 64, 183
- Bhatia, A. K., Doschek, G. A., & Eissner, W. 2002, At. Data Nucl. Data Tables, 82, 211
- Brosius, J. W., Davila, J. M., Thomas, R. J., & Monsignori-Fossi, B. C. 1996, ApJS, 106, 143
- Brosius, J. W., Davila, J. M., & Thomas, R. J. 1998, ApJS, 119, 255
- Deb, N. C., & Tayal, S. S. 1998, At. Data Nucl. Data Tables, 69, 161
- Dere, K. P. 1978, ApJ, 221, 1062
- Dere, K. P., Landi, E., Mason, H. E., Monsignori-Fossi, B. C., & Young, P. R. 1997, A&AS, 125, 149
- Dufton, P. L. 1977, Comp. Phys. Commun., 13, 25
- Dufton, P. L., Berrington, K. A., Burke, P. G., & Kingston, A. E. 1978, A&A, 62, 111
- Dufton, P. L., Kingston, A. E., Doyle, J. G., & Widing, K. G. 1983, MNRAS, 205, 81
- Gupta, G. P., & Tayal, S. S. 1999a, ApJ, 510, 1078
- Gupta, G. P., & Tayal, S. S. 1999b, ApJS, 123, 295
- Howarth, I. D., Murray, J., & Mills, D. 1994, Starlink User Note No. 50.15
- Jupén, C., Isler, R. C., & Träbert, E. 1993, MNRAS, 264, 627
- Kastner, S. O., & Mason, H. E. 1978, A&A, 67, 119
- Keenan, F. P., Aggarwal, K. M., Katsiyannis, A. C., & Reid, R. H. G. 2003, Sol. Phys., 217, 225

- Keenan, F. P., Botha, G. J. J., Matthews, A., Lawson, K. D., & Coffey, I. H. 2000, *MNRAS*, 318, 37
- Kelly, R. L. 1987, *J. Phys. Chem. Ref. Data*, 16, Suppl. 1
- Landman, D. A. 1980, *ApJ*, 240, 709
- Mazzotta, P., Mazzitelli, G., Colafrancesco, S., & Vittorio, N. 1998, *A&AS*, 133, 403
- Neupert, W. M., Epstein, G. L., Thomas, R. J., & Thompson, W. T. 1992, *Sol. Phys.*, 137, 87
- Shirai, T., Funatake, Y., Mori, K., Sugar, J., Wiese, W. L., & Nakai, Y. 1990, *J. Phys. Chem. Ref. Data*, 19, 127
- Thomas, R. J., & Neupert, W. M. 1994, *ApJS*, 91, 461
- Young, P. R., Del Zanna, G., Landi, E., Dere, K. P., Mason, H. E., & Landini, M. 2003, *ApJS*, 144, 135

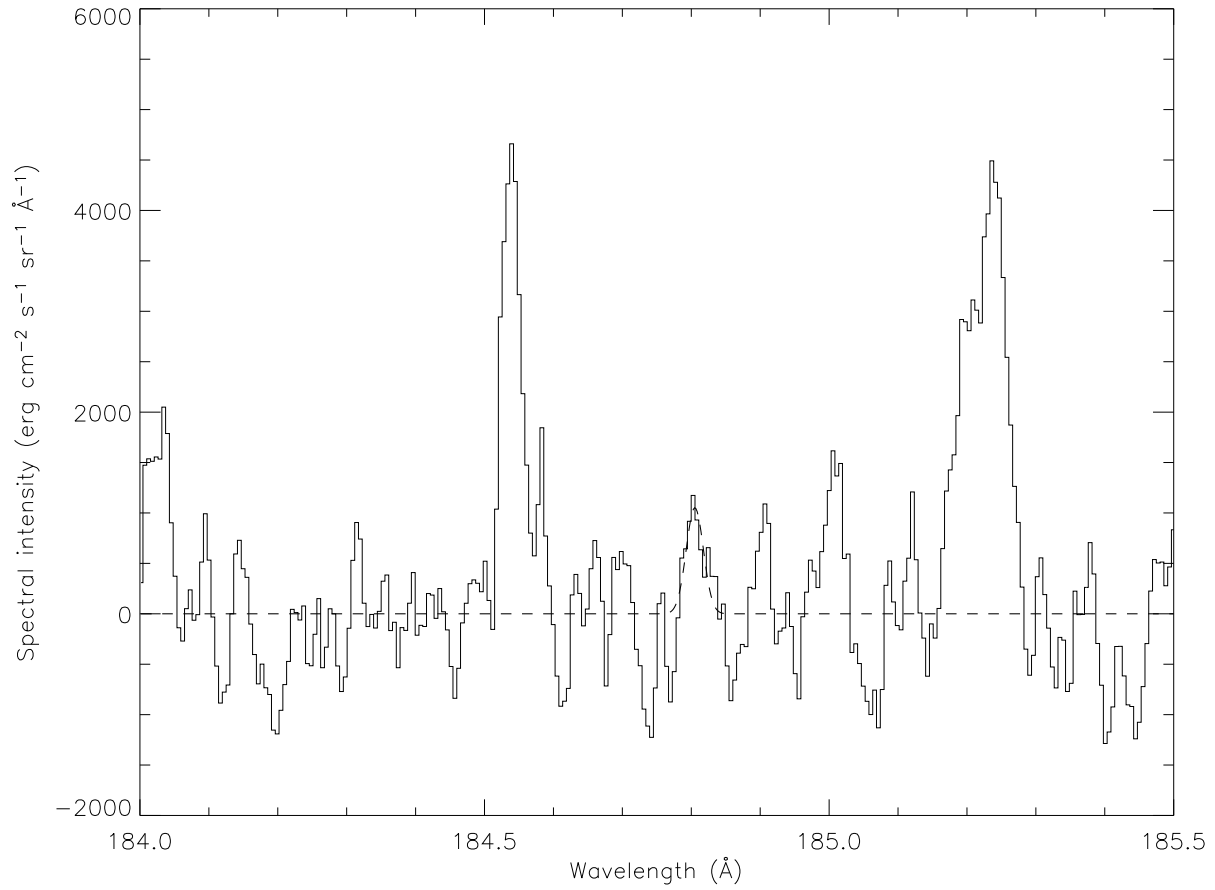


Fig. 1.— Plot of the SERTS 1995 active region spectrum in the 184.0–185.5 Å wavelength range. The profile fit to the Fe XI 184.80 Å feature is shown by a dashed line. Also clearly visible in the figure are the Fe X 184.53 Å and Fe VIII/Ni XVI 185.22 Å lines.

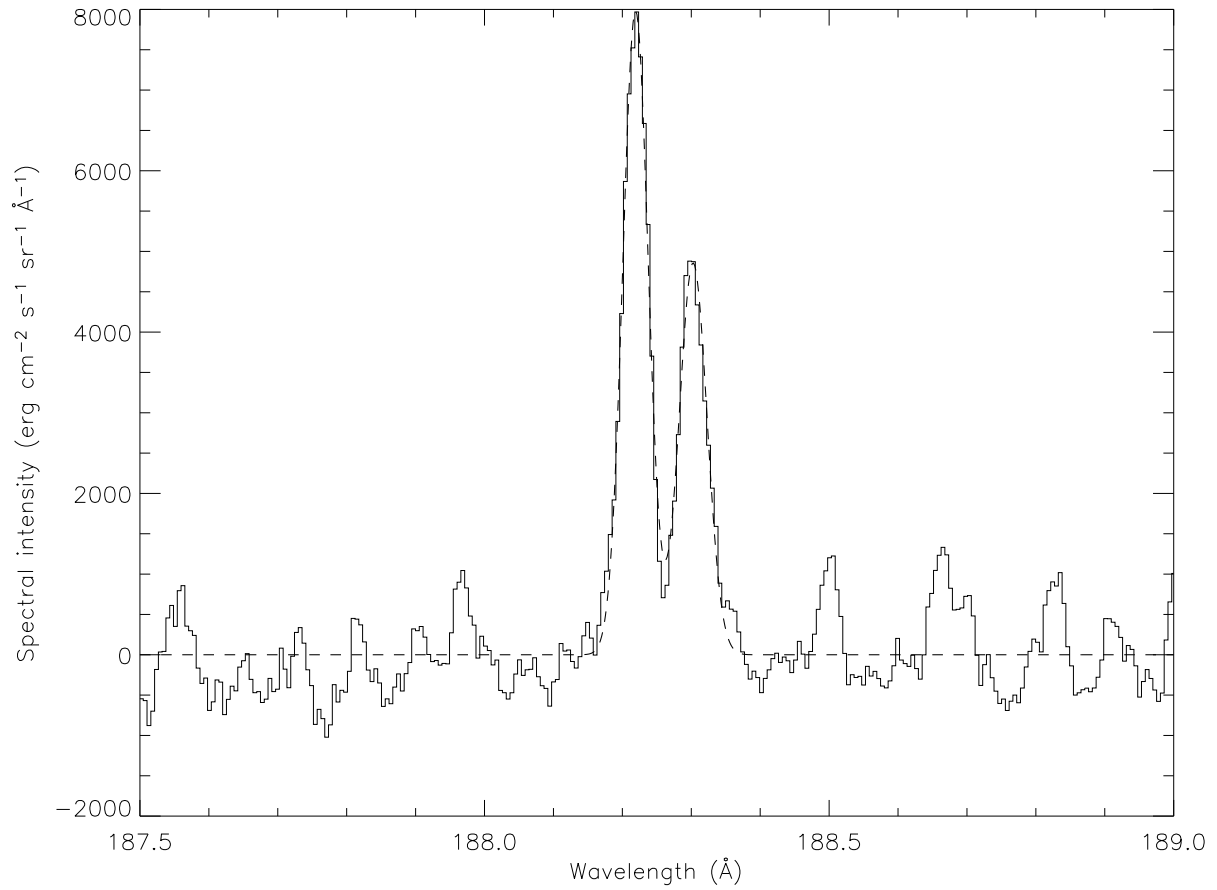


Fig. 2.— Plot of the SERTS 1995 active region spectrum in the 187.5–189.0 Å wavelength range. The profile fit to the Fe XI 188.21 and 188.30 Å features is shown by a dashed line. Also clearly visible in the figure are the S XI 188.66 Å and Ar XI 188.82 Å lines.

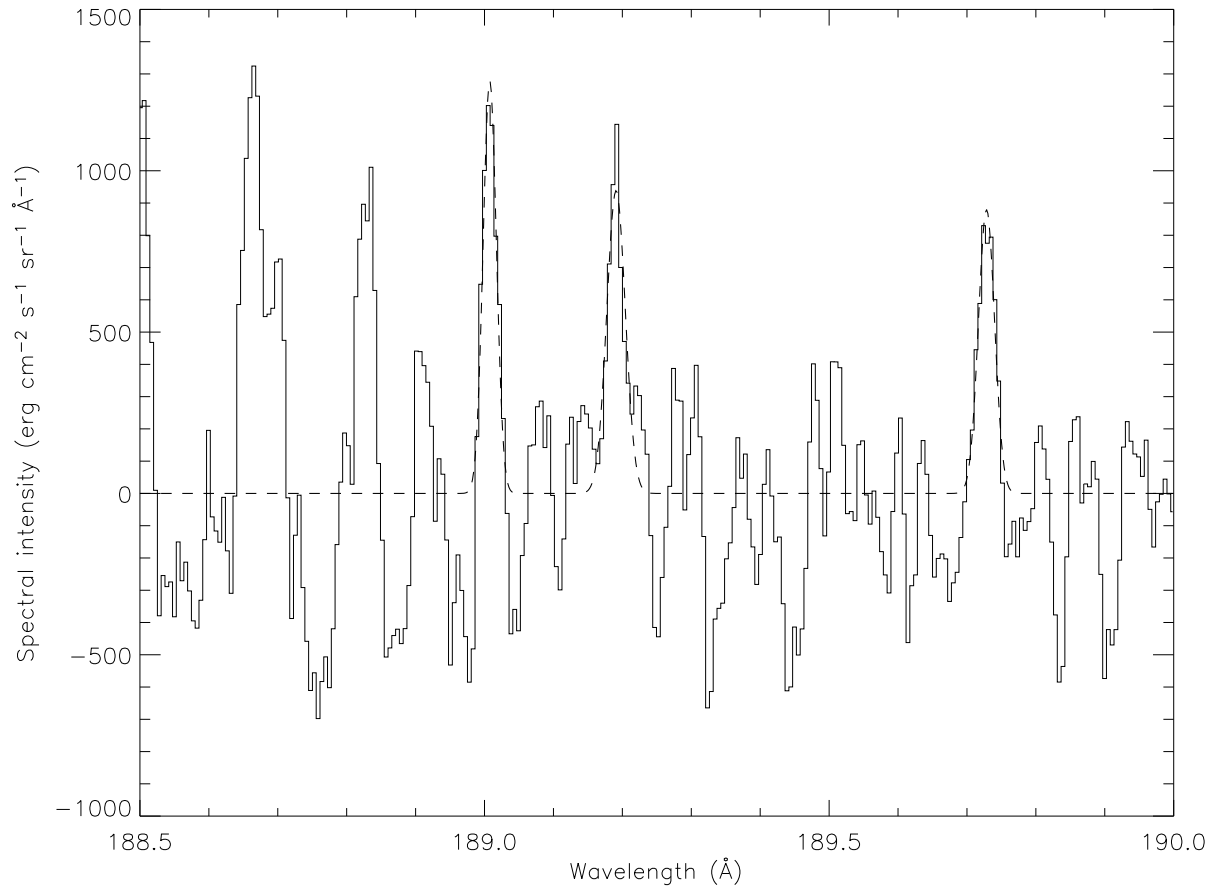


Fig. 3.— Plot of the SERTS 1995 active region spectrum in the 188.5–190.0 Å wavelength range. The profile fit to the Fe XI 189.00, 189.19 and 189.72 Å features is shown by a dashed line. Also clearly visible in the figure are the S XI 188.66 Å and Ar XI 188.82 Å lines.

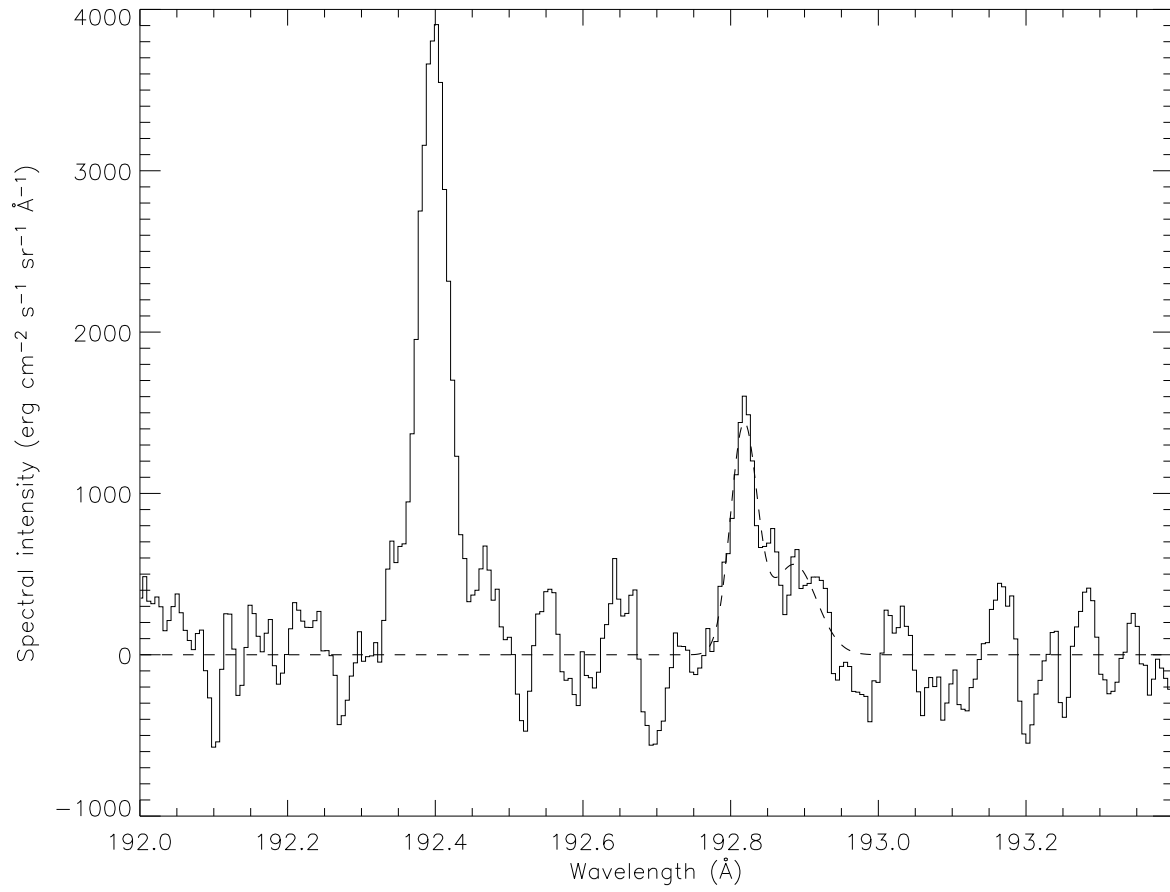


Fig. 4.— Plot of the SERTS 1995 active region spectrum in the 192.0–193.4 Å wavelength range. The profile fit to the Fe XI 192.81 and 192.88 Å features is shown by a dashed line. Also clearly visible in the figure is the Fe XII 192.39 Å line.

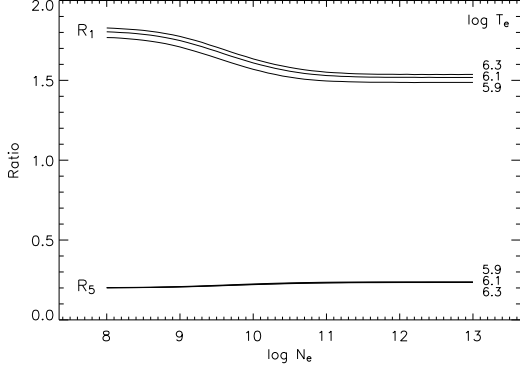


Fig. 5.— The theoretical Fe XI emission line intensity ratios  $R_1 = I(180.38 \text{ \AA})/I(188.21 \text{ \AA})$  and  $R_5 = I(188.30 \text{ \AA})/I(188.21 \text{ \AA})$ , where  $I$  is in energy units, plotted as a function of logarithmic electron density ( $N_e$  in  $\text{cm}^{-3}$ ) at the temperature of maximum Fe XI fractional abundance in ionization equilibrium,  $T_e = 10^{6.1}$  K (Mazzotta et al. 1998), plus  $\pm 0.2$  dex about this value.

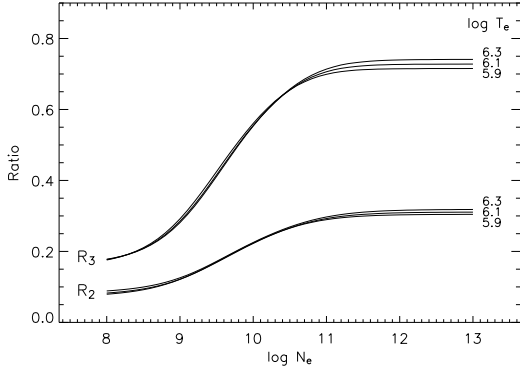


Fig. 6.— The theoretical Fe XI emission line intensity ratios  $R_2 = I(181.13 \text{ \AA})/I(188.21 \text{ \AA})$  and  $R_3 = I(182.17 \text{ \AA})/I(188.21 \text{ \AA})$ , where  $I$  is in energy units, plotted as a function of logarithmic electron density ( $N_e$  in  $\text{cm}^{-3}$ ) at the temperature of maximum Fe XI fractional abundance in ionization equilibrium,  $T_e = 10^{6.1}$  K (Mazzotta et al. 1998), plus  $\pm 0.2$  dex about this value.

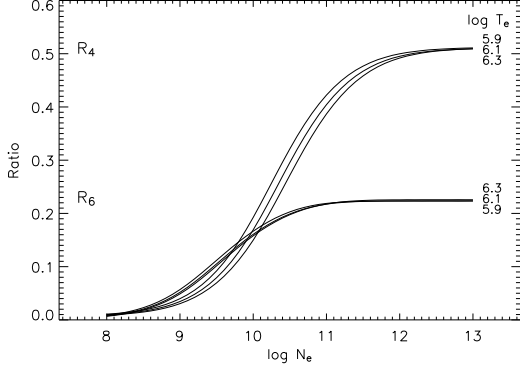


Fig. 7.— The theoretical Fe XI emission line intensity ratios  $R_4 = I(184.80 \text{ \AA})/I(188.21 \text{ \AA})$  and  $R_6 = I(189.00 \text{ \AA})/I(188.21 \text{ \AA})$ , where  $I$  is in energy units, plotted as a function of logarithmic electron density ( $N_e$  in  $\text{cm}^{-3}$ ) at the temperature of maximum Fe XI fractional abundance in ionization equilibrium,  $T_e = 10^{6.1} \text{ K}$  (Mazzotta et al. 1998), plus  $\pm 0.2$  dex about this value.

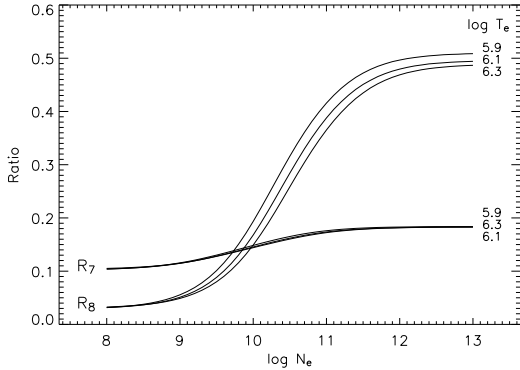


Fig. 8.— The theoretical Fe XI emission line intensity ratios  $R_7 = I(189.19 \text{ \AA})/I(188.21 \text{ \AA})$  and  $R_8 = I(202.42 \text{ \AA})/I(188.21 \text{ \AA})$ , where  $I$  is in energy units, plotted as a function of logarithmic electron density ( $N_e$  in  $\text{cm}^{-3}$ ) at the temperature of maximum Fe XI fractional abundance in ionization equilibrium,  $T_e = 10^{6.1} \text{ K}$  (Mazzotta et al. 1998), plus  $\pm 0.2$  dex about this value.

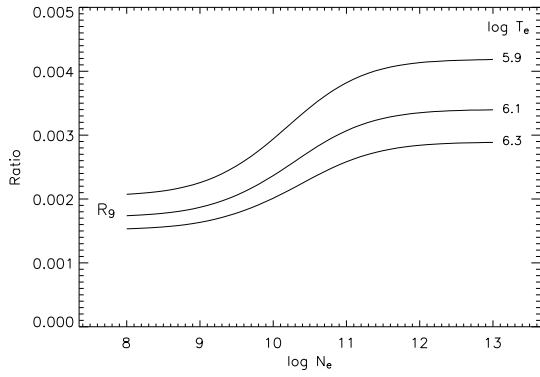


Fig. 9.— The theoretical Fe XI emission line intensity ratio  $R_9 = I(223.00 \text{ \AA})/I(188.21 \text{ \AA})$ , where  $I$  is in energy units, plotted as a function of logarithmic electron density ( $N_e$  in  $\text{cm}^{-3}$ ) at the temperature of maximum Fe XI fractional abundance in ionization equilibrium,  $T_e = 10^{6.1} \text{ K}$  (Mazzotta et al. 1998), plus  $\pm 0.2$  dex about this value.

Table 1. Fe XI line identifications in the SERTS 1995 active region spectrum

Wavelength (Å)	Transition	Note <sup>a</sup>
180.38	$3s^23p^4\ ^3P_2-3s^23p^3(^4S)3d\ ^3D_3$	Blended with first-order Fe XVI line
181.13	$3s^23p^4\ ^3P_0-3s^23p^3(^4S)3d\ ^3D_1$	...
182.17	$3s^23p^4\ ^3P_1-3s^23p^3(^4S)3d\ ^3D_2$	...
184.80	$3s^23p^4\ ^1D_2-3s^23p^3(^2D)3d\ ^1D_2$	...
188.21	$3s^23p^4\ ^3P_2-3s^23p^3(^2D)3d\ ^3P_2$	...
188.30	$3s^23p^4\ ^3P_2-3s^23p^3(^2D)3d\ ^3S_1$	Tentative identification as Fe XI
189.00	$3s^23p^4\ ^3P_1-3s^23p^3(^2D)3d\ ^3P_0$	Unidentified
189.19	$3s^23p^4\ ^3P_1-3s^23p^3(^2D)3d\ ^3P_1$	Tentative identification as Fe XI
189.72	$3s^23p^4\ ^3P_0-3s^23p^3(^2D)3d\ ^3P_1$	...
192.81	$3s^23p^4\ ^3P_1-3s^23p^3(^2D)3d\ ^3P_2$	...
192.88	$3s^23p^4\ ^3P_1-3s^23p^3(^2D)3d\ ^3S_1$	Listed as Ca XVII
193.51	$3s^23p^4\ ^3P_0-3s^23p^3(^2D)3d\ ^3S_1$	Listed as Fe XII
198.56	$3s^23p^4\ ^1D_2-3s^23p^3(^2D)3d\ ^3P_1$	Listed as S VIII/Fe XII blend
202.42	$3s^23p^4\ ^1D_2-3s^23p^3(^2D)3d\ ^1P_1$	Listed as Fe XIII
223.00	$3s^23p^4\ ^1D_2-3s^23p^3(^2P)3d\ ^3D_1$	Listed as Fe XI/Ca XVII blend

<sup>a</sup>From Brosius et al. (1998).

Table 2. Fe XI line intensities and widths in the SERTS 1995 active region spectrum

Wavelength (Å)	Intensity <sup>a</sup>	Line width (Å)
180.38	3474 ± 384.5	0.051 ± 0.003
181.13	123.8 ± 35.3	0.054 ± 0.011
182.17	231.5 ± 31.6	0.038 ± 0.004
184.80	32.9 ± 11.8	0.029 ± 0.009
188.21	369.1 ± 68.5	0.043 ± 0.006
188.30	245.9 ± 44.8	0.048 ± 0.007
189.00	30.8 ± 8.0	0.023 ± 0.004
189.19	31.6 ± 8.5	0.032 ± 0.006
189.72	25.9 ± 6.3	0.028 ± 0.005
192.81	68.4 ± 9.5	0.043 ± 0.004
192.88	38.5 ± 10.0	0.072 ± 0.014
193.51	478.8 ± 54.6	0.049 ± 0.003
198.56	52.0 ± 10.2	0.036 ± 0.005
202.42	71.2 ± 16.8	0.032 ± 0.005
223.00	78.2 ± 16.3	0.029 ± 0.004

<sup>a</sup>In erg cm<sup>-2</sup> s<sup>-1</sup> sr<sup>-1</sup>.

Table 3. Fe XI line ratios in the SERTS 1995 active region spectrum

Line ratio	Observed	Theoretical <sup>a</sup>
$R_1 = I(180.38 \text{ \AA})/I(188.21 \text{ \AA})$	$9.4 \pm 2.0$	$1.7 \pm 0.3$
$R_2 = I(181.13 \text{ \AA})/I(188.21 \text{ \AA})$	$0.34 \pm 0.12$	$0.16 \pm 0.03$
$R_3 = I(182.17 \text{ \AA})/I(188.21 \text{ \AA})$	$0.63 \pm 0.15$	$0.39 \pm 0.08$
$R_4 = I(184.80 \text{ \AA})/I(188.21 \text{ \AA})$	$0.089 \pm 0.036$	$0.067 \pm 0.013$
$R_5 = I(188.30 \text{ \AA})/I(188.21 \text{ \AA})$	$0.67 \pm 0.17$	$0.21 \pm 0.04$
$R_6 = I(189.00 \text{ \AA})/I(188.21 \text{ \AA})$	$0.083 \pm 0.026$	$0.093 \pm 0.019$
$R_7 = I(189.19 \text{ \AA})/I(188.21 \text{ \AA})$	$0.086 \pm 0.028$	$0.13 \pm 0.03$
$R_{10} = I(189.72 \text{ \AA})/I(188.21 \text{ \AA})$	$0.070 \pm 0.021$	$0.11 \pm 0.02$
$R_{14} = I(192.81 \text{ \AA})/I(188.21 \text{ \AA})$	$0.19 \pm 0.04$	$0.19 \pm 0.04$
$R_{11} = I(192.88 \text{ \AA})/I(188.21 \text{ \AA})$	$0.10 \pm 0.03$	$0.072 \pm 0.014$
$R_{12} = I(193.51 \text{ \AA})/I(188.21 \text{ \AA})$	$1.3 \pm 0.3$	$0.020 \pm 0.004$
$R_{13} = I(198.56 \text{ \AA})/I(188.21 \text{ \AA})$	$0.14 \pm 0.04$	$0.055 \pm 0.011$
$R_8 = I(202.42 \text{ \AA})/I(188.21 \text{ \AA})$	$0.19 \pm 0.06$	$0.078 \pm 0.016$
$R_9 = I(223.00 \text{ \AA})/I(188.21 \text{ \AA})$	$0.21 \pm 0.06$	$0.0020 \pm 0.0004$

<sup>a</sup>Determined from Figures 5–9 at  $N_e = 10^{9.4} \text{ cm}^{-3}$ .